Water Science and Engineering, 2009, 2(1): 74-85
doi:10.3882/j.issn.1674-2370.2009.01.007

http://kkb.hhu.edu.cn
e-mail: wse@hhu.edu.cn

Numerical simulation of transient flow in horizontal drainage systems

Ze-yu MAO*, Han XIAO, Ying LIU, Ying-jun HU

Department of Hydraulic Engineering, Tsinghua University, Beijing 100084, P. R. China

Abstract: A numerical simulation model based on the characteristic-based finite-difference method with a time-line interpolation scheme was developed for predicting transient free surface flow in horizontal drainage systems. The fundamental accuracy of the numerical model was first clarified by comparison with the experimental results for a single drainage pipe. Boundary conditions for junctions and bends, which are often encountered in drainage systems, were studied both experimentally and numerically. The numerical model was applied to an actual drainage system. Comparison with a full-scale model experiment indicates that the model can be used to accurately predict flow characteristics in actual drainage networks.

Key words: *transient flow; drainage systems; time-line interpolation; urbanization*

1 Introduction

Accurately modeling wave attenuation in drainage networks is advantageous in allowing the prediction of the effects of wave attenuation on solid transport, drainage capacity, maximum flow depth, pressure transients, mass or surge oscillations and maintenance. The current trend towards water conservation will make it even more important to accurately estimate flow attenuation (Swaffield and Galowin 1992; Mao 1993; Mao 1995; Mao and Chen 1997; Mao et al. 2004).

Consideration of distinct characteristics of transient flow in drainage systems contributes to both the selection of numerical techniques requiring small computational time steps and the choice of a numerical method that allows the accurate representation of a system with complicated boundary conditions. In this paper, a one-dimensional numerical model of transient flow for horizontal drainage systems is described.

2 Numerical model

The following equations were used to develop the numerical model:

$$T\frac{\partial h}{\partial t}+A\frac{\partial V}{\partial x}+VT\frac{\partial h}{\partial x}=0 \tag{1}$$

This work was supported by the National Natural Science Foundation of China (Grant No. 50879035).
*Corresponding author (e-mail: *maozeyu@tsinghua.edu.cn*)
Received Dec. 31, 2008; accepted Feb. 17, 2009

$$\frac{1}{g}\frac{\partial V}{\partial t}+\frac{V}{g}\frac{\partial V}{\partial x}+\frac{\partial h}{\partial x}+S_{\mathrm{f}}-S_0=0 \tag{2}$$

where h is the water depth; A is the flow cross section area; T is the surface width of flow; V is the mean velocity, defined as $V=Q/A$, with Q being the discharge; g is the acceleration due to gravity; S_{f} is the friction slope; and S_0 is the pipe slope.

The characteristic-based finite-difference method with space-line interpolation, as shown in Fig. 1, has been used widely. However, the solution procedure has been found to inherently produce artificial numerical damping and dispersion, causing the wave front to seriously flatten (Mao 1993). Time-line interpolation has been recommended as an alternative (Fig. 2). Comprehensive stability and error analysis and comparisons with other numerical methods have been presented in detail by Mao (1993) and She and Mao (2003).

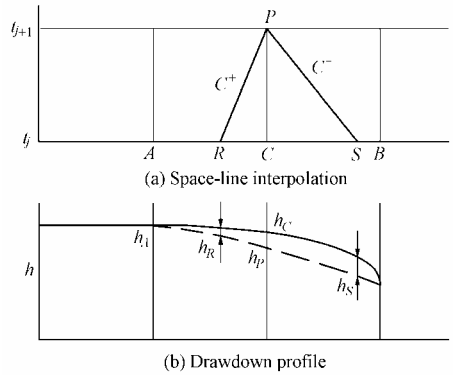

Fig. 1 Space-line interpolation error of gradually varied flow

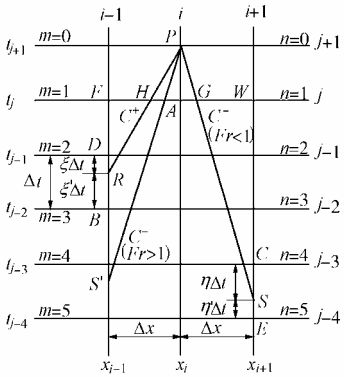

Fig. 2 Time-line interpolation

The following four algebraic equations arise from a first-order approximation:

For positive characteristic line C^+,

$$V_P-V_R+\frac{g}{C_R}(h_P-h_R)+g(S_{\mathrm{f}R}-S_0)(t_P-t_R)=0 \tag{3}$$

$$x_P-x_R-(V_R+C_R)(t_P-t_R)=0 \tag{4}$$

For negative characteristic line C^-,

$$V_P-V_S-\frac{g}{C_S}(h_P-h_S)+g(S_{\mathrm{f}S}-S_0)(t_P-t_S)=0 \tag{5}$$

$$x_P-x_S-(V_S-C_S)(t_P-t_S)=0 \tag{6}$$

where C is the wave propagation velocity, defined as $C=\sqrt{\dfrac{gA}{T}}$; and the subscripts represent the different points shown in Fig. 2.

The interpolation algorithm can be formulated based on a first-degree Lagrangian polynomial:

$$f_R=\xi f_D+\xi' f_B,\qquad \xi=\frac{x_i-x_{i-1}}{(t_{j-1}-t_{j-2})(V_R+C_R)}-\frac{t_{j+1}-t_{j-1}}{t_{j-1}-t_{j-2}},\qquad \xi'=1-\xi \tag{7}$$

$$f_S = \eta\, f_E + \eta' f_C\,, \qquad \eta = \frac{x_{i+1} - x_i}{(t_{j-3} - t_{j-4})\,(V_S + C_S)} - \frac{t_{j+1} - t_{j-3}}{t_{j-3} - t_{j-4}}\,, \qquad \eta' = 1 - \eta \tag{8}$$

where *f* is the variable of interest, either *h*, *V*, or *C*. The values of V_R, h_R and C_R for the C^+ line can be obtained through simultaneous solution of Eq. (7). In a similar fashion, the values of V_S, h_S and C_S for the C^- line of subcritical flow are obtained through solution of Eq. (8). A similar procedure can be used to derive the expression for the C^- line of supercritical flow.

The time interval of the intersection point *R* (Fig. 2) can be obtained by solving the following equation:

$$F_R(\xi) = \frac{t_P - \left[t_B - \xi\left(t_B - t_D\right)\right]}{x_i - x_{i-1}} - \frac{1}{\xi\,\left(V_D + C_D\right) + \left(1 - \xi\right)\left(V_B + C_B\right)} = 0 \tag{9}$$

at the time interval's boundary node:

$$\begin{cases} F_R(\xi = 0) = \dfrac{t_P - t_B}{x_i - x_{i-1}} - \dfrac{1}{V_B + C_B} = F_{RB} \\ F_R(\xi = 1) = \dfrac{t_P - t_D}{x_i - x_{i-1}} - \dfrac{1}{V_D + C_D} = F_{RD} \end{cases} \tag{10}$$

The time intervals t_B and t_D are determined by comparing the signs of F_{RB} and F_{RD}. The time intervals t_C and t_E can be determined in a similar way. Thus, flow depth and velocity along a pipe over any time range can be determined through systematic application and solution of the characteristic equations beginning with a known initial flow condition at time zero. The Courant stability criteria governs the time step Δt:

$$\Delta t \;\le\; \frac{\Delta x}{\left(|V| + C\right)_{\max}} \tag{11}$$

By solving the available C^+ equation (Eq. (3)) or C^- equation (Eq. (5)) with appropriate flow-describing equations, the boundary conditions can be modeled (Mao 1993).

3 Numerical model verification for single pipe

In order to verify the adequacy of the presented numerical model for modeling circular pipe flow, a numerical test was conducted for the experimental case shown in Fig. 3. A circular PVC pipe (CP) with a length of 35 m and a diameter of 100 cm was used to generate comparative data to check the fundamental accuracy of the prediction method. Outflow from the main pipe exited via a vented tee-piece and flowed through another PVC pipe back to the storage tank, where the water could be re-circulated. In the same manner as the internal nodes, the exit boundary conditions for supercritical flow were determined by simultaneous solution of the positive and negative characteristic lines. The initial flow rate was set at 0.1 cm^3/s, and Manning's loss coefficient was 0.008 7 (an experimentally determined value). The observed and predicted depth variations at points *A* through *E* are shown in Fig. 4. The agreement between the observed and predicted depths was excellent.

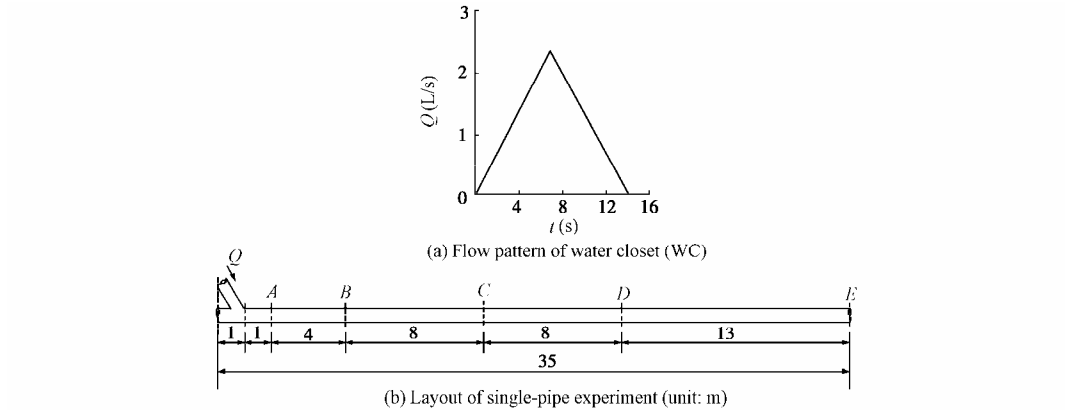

Fig. 3 Sketch of single-pipe experimental device with slope of 1/100

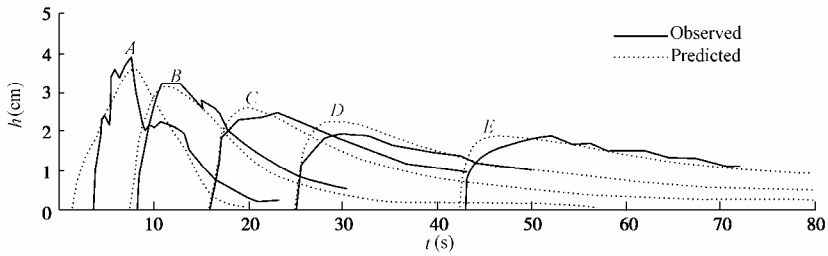

Fig. 4 Comparison of observed and predicted depths

4 Study on water flow through junctions

4.1 Moving hydraulic jump model

In order to expand the applicability of the method of characteristics from a single pipe to a drainage system, the model must be capable of modeling the attenuation of flow profiles as they pass through junctions. Accurate simulation of junction conditions is an essential part of a partially filled pipe network model and is of particular importance in drainage networks due to the relatively small pipe diameter and short runs between internal boundaries. The following model is based upon the premise that the flow in the pipes leading to the junction is supercritical due to the effect of a steep slope. The flow profiles surrounding a junction is shown in Fig. 5, in which Q_d is the downstream combined discharge, Q_m is the main pipe discharge, h_j is the junction depth, h_c is the critical depth of combined discharge, h_u is the normal depth of main pipe flow, and h_d is the normal depth of downstream combined discharge.

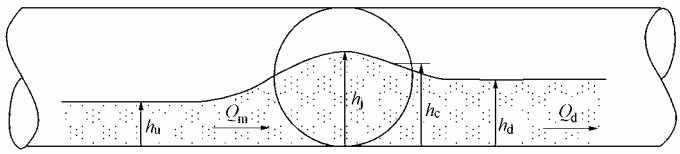

Fig. 5 Flow profiles surrounding junction

As shown in Fig. 6(a), by superposing the reversed velocity of traveling jump V_w on the system, the free surface boundary can be brought to rest. Applying the continuity and momentum principles across the jump, we have

$$(V_1 - V_w) A_1 = (V_2 - V_w) A_2 \tag{12}$$

$$gA_1\bar{h}_1 - gA_2\bar{h}_2 = A_2 (V_2 - V_w)^2 - A_1 (V_1 - V_w)^2 \tag{13}$$

where A_1 and A_2 are the areas of cross sections upstream and downstream of the jump, respectively; $\bar{h}_1$ and $\bar{h}_2$ are the depths to the centroids of cross sections upstream and downstream of the jump, respectively; and V_1 and V_2 are the mean velocity at cross sections upstream and downstream of the jump, respectively. Therefore, the velocity of the traveling jump V_w and the flow conditions both upstream (velocity V_1 and depth h_1) and downstream (velocity V_2 and depth h_2) of the jump at each time step are determined by simultaneously solving these two equations, together with the C^+ and C^- equations for upstream supercritical flow and the C^- equation for downstream subcritical flow (Fig. 6(b)) (Mao 1996a, 1996c).

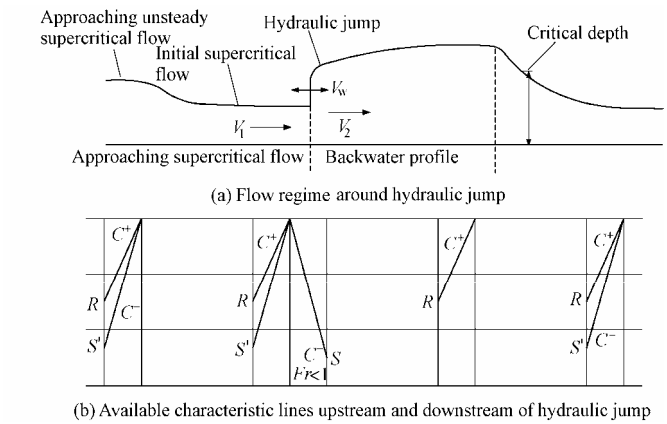

Fig. 6 Sketch of numerical simulation of moving hydraulic jump

4.2 Junction depth formulae

The numerical model of unsteady flow through a junction requires supplementary information about the junction, i.e. the appropriate junction depth must be estimated at each simulation time step. These junction boundary conditions can also be used to predict the limiting discharge capacity. The development of the junction boundary conditions is dependent upon the investigated flow properties, and different flow patterns will certainly result in different empirical equations (Mao 1996b).

Detailed measurements around junctions were made under steady state conditions. The rotameters in both the main pipe, with a diameter of 100 cm (CP 100), and the branch pipe, with a diameter of 75 cm (CP 75), had a measurement range of 0.1-13 L/s. The experimental

device and conditions are shown in Fig. 7.

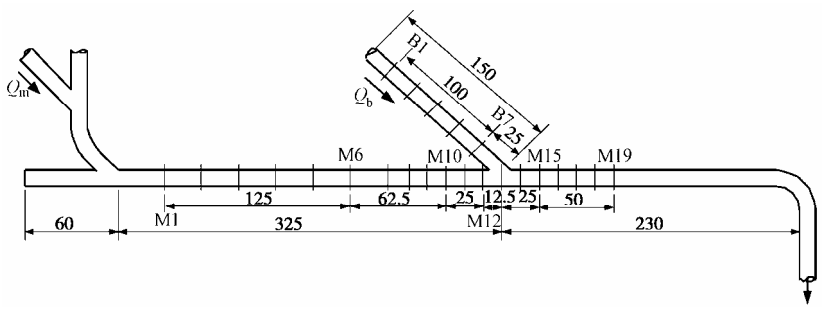

Fig. 7 Sketch of experimental device and conditions (Unit: cm)

The experimental results yielded the empirical relationships between the junction depth and the combined flow rate, as shown in Fig. 8:

For a 90° junction,

$$R_h = -1.145\left(1-R_Q\right)^{3.627} + 2.072 \tag{14}$$

For a 45° junction,

$$R_h = 1.019\,8 + 3.190\,7\,R_Q - 2.779\,7R_Q^{\,2} \tag{15}$$

where the depth ratio $R_h = h_j/h_d$, the discharge ratio $R_Q = Q_b/\left(Q_m + Q_b\right)$, and Q_b is the branch pipe discharge.

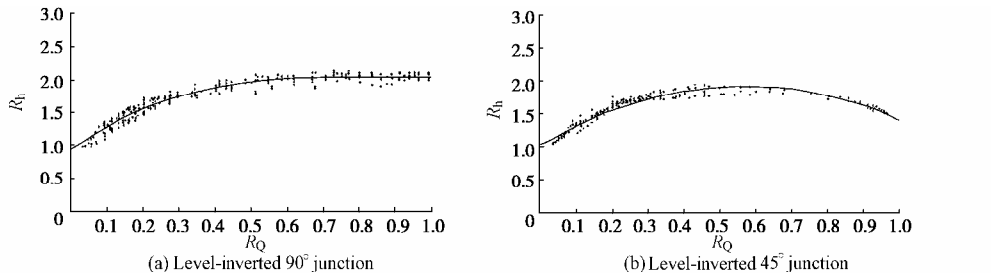

Fig. 8 Junction depth ratio vs. discharge ratio

4.3 Study of unsteady flow through junction

4.3.1 Junction model

Flow is impeded by pipe junctions, causing a region of subcritical flow. Thus, only the C^+ equation (Eq. (3)) exists at the final node. The junction model can be developed based on the present numerical model and appropriate junction depth formulae (Eqs. (14) and (15)). Therefore, under the assumption that the depths at the junctions of all connecting pipes are equal, simultaneous solution of the junction depth formulae with the C^+ equations for all the joining pipes allows the solution to proceed.

4.3.2 Model validation

Fig. 9 shows the entry form of the branch pipe for unsteady flow. Setting the steady flow rate of the main pipe to 1 L/s or 0.5 L/s, water reserved in a washing sink was discharged into

the branch pipe at the steady flow rate of 0.17 L/s.

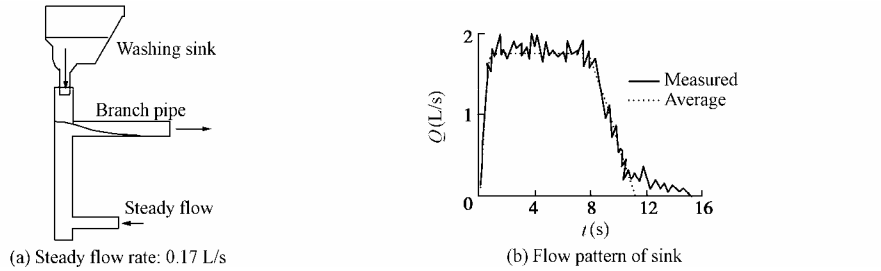

Fig. 9 Entry form of branch pipe for unsteady flow

The flow depth was measured at eight points: M1, M6, M10, M12, M15, M19, B1, and B7, all shown in Fig. 7 with resistant wire-type water height meters. The pipe route was divided into three elements: the upstream and downstream sides of the main pipe and the branch pipe at the junction point. Numerical simulation was conducted separately for each flow element.

Figs. 10 and 11 show the comparison of simulated and measured depths at four typical measurement points when the steady flow rate of the main pipe is 1.0 L/s and 0.5 L/s, respectively. The simulated results showed fairly good agreement with the measured results.

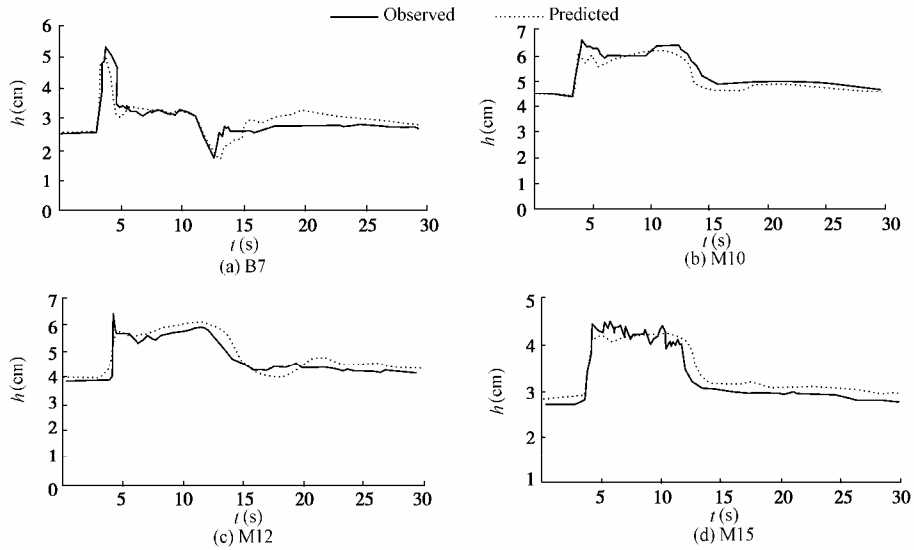

Fig. 10 Comparison of observed and predicted depths of unsteady flow at four measurement points (steady flow rate of main flow: 1.0 L/s)

5 Bend model

In order to predict the entire flow in horizontal drainage systems, the bends also need to be modeled. By applying steady flow to pipes with bends of 45° and 90°, the spatial variation of the depth was measured. The experimental device and conditions are shown in Fig. 12.

Bend effects may be accounted for by imposing proper flow resistance distribution in the

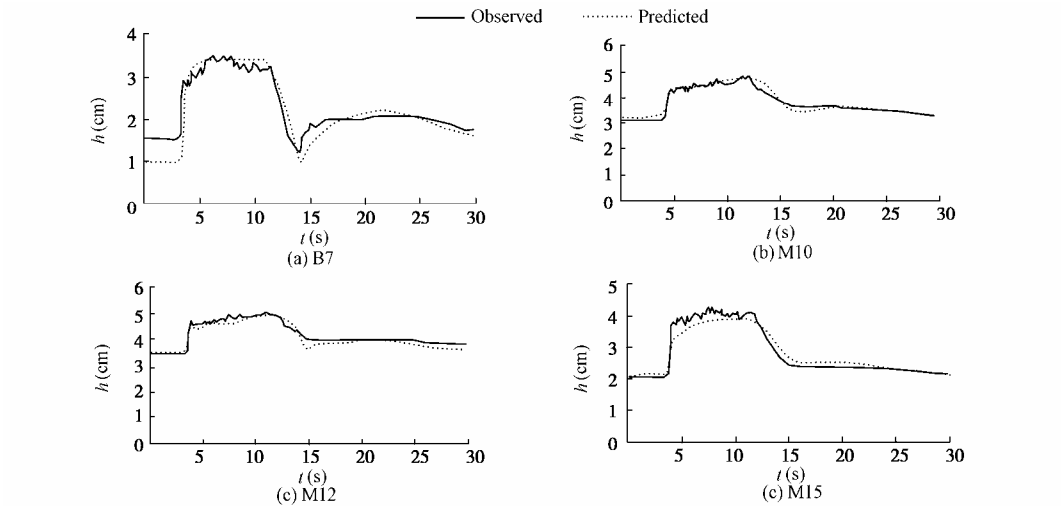

Fig. 11 Comparison of observed and predicted depths of unsteady flow at four measurement points (steady flow rate of main flow: 0.5 L/s)

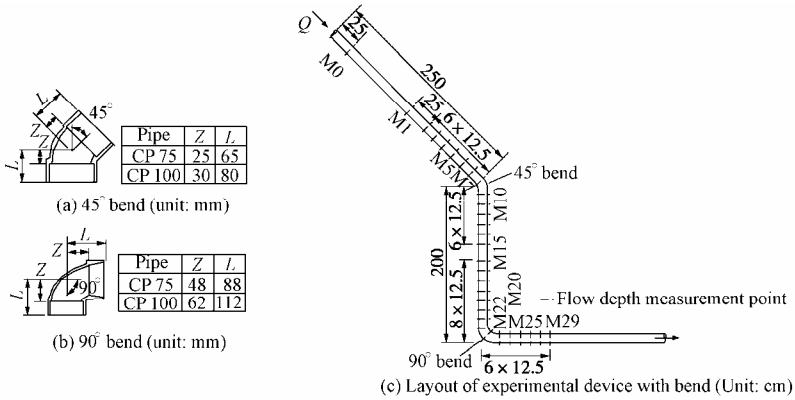

Fig. 12 Sketch of experimental device and conditions of bend model

single pipe flow calculation. The flow resistance coefficient is now interpreted as being composed of the wall resistance coefficient and the bend loss coefficient at the corresponding locations. The bend loss coefficient was obtained by integrating the momentum equation (Eq. 2) over a finite flow domain $x_1 - x_2$, which included bends (Fig. 13), and omitting the time derivation term under the assumption of steady state conditions:

$$\Delta n = \sqrt{\frac{R_{ab}^{4/3} A_{ab}^2}{gQ^2(x_2 - x_1)}\left[\left(\frac{Q^2}{A^2} + \frac{p}{\rho g}\right)_{x_1} - \left(\frac{Q^2}{A^2} + \frac{p}{\rho g}\right)_{x_2} - gn^2Q^2\int_{x_1}^{x_2}\frac{1}{R^{4/3}A^2}\mathrm{d}x + gS_0(x_2 - x_1)\right]} \quad (16)$$

where Δn is the bend loss coefficient, R_{ab} is the average hydraulic radius of the bend, A_{ab} is the average cross sectional area of the bend, n is the Manning's roughness, p is the water pressure, R is the hydraulic radius of the pipe, and ρ is the water density.

Measured data were then substituted into the equation, changing the integration domain for 45° and 90° bends. The estimated bend loss coefficients for pipes with slopes of both 1/50 and 1/100 and bends of 45° and 90° are shown in Fig. 14 as a function of the flow rate.

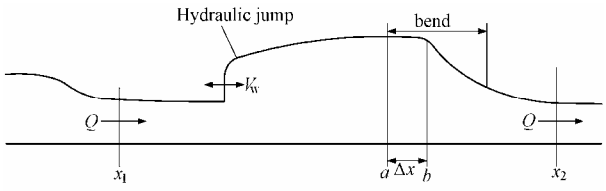

Fig. 13 Flow regime around bend

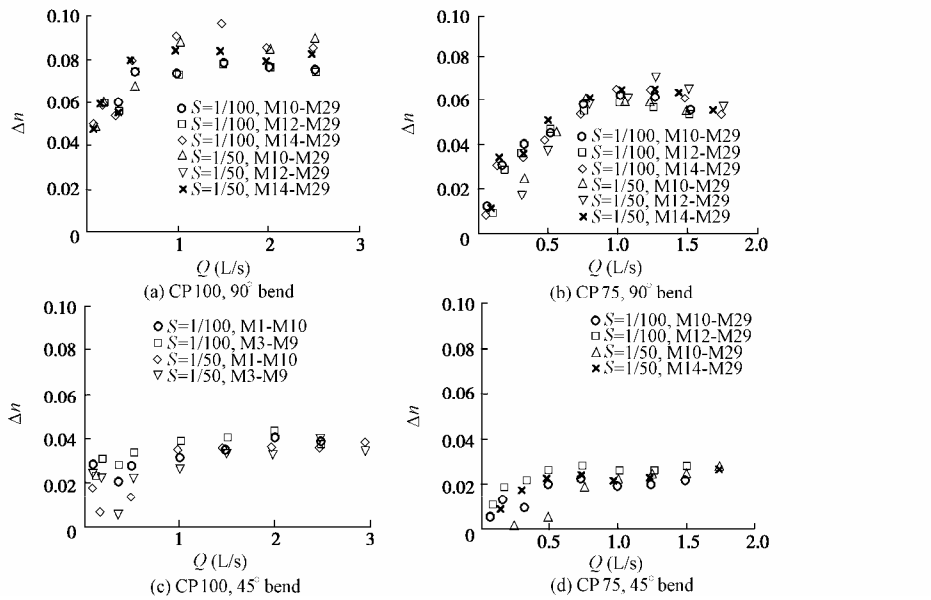

Fig. 14 Calculated bend loss coefficients

These figures indicate that the integration domain and the pipe slope have little influence on the estimated coefficient, and the loss coefficient tends to decrease below 0.5 L/s, while it is nearly constant above 0.75 L/s. Since the bend effect seems significant for a relatively large flow rate, the experimental data above 0.5 L/s were averaged, and the average was used as a bend loss coefficient in each case.

Using the experimental device given in Fig. 12, unsteady flow was applied to the upstream end by the washing sink shown in Fig. 9. There were thirty flow depth measurement points: M0, M1, ⋯, and M29, shown in Fig. 12.

Figs. 15 and 16 show the comparisons of simulated and measured results for the pipes with slopes of 1/50 and 1/100, respectively, at six typical measurement points influenced by the bends. The simulated results are generally in agreement with the experimental results, though some discrepancies are apparent. The presented bend model seems acceptable when

the practical applications are concerned.

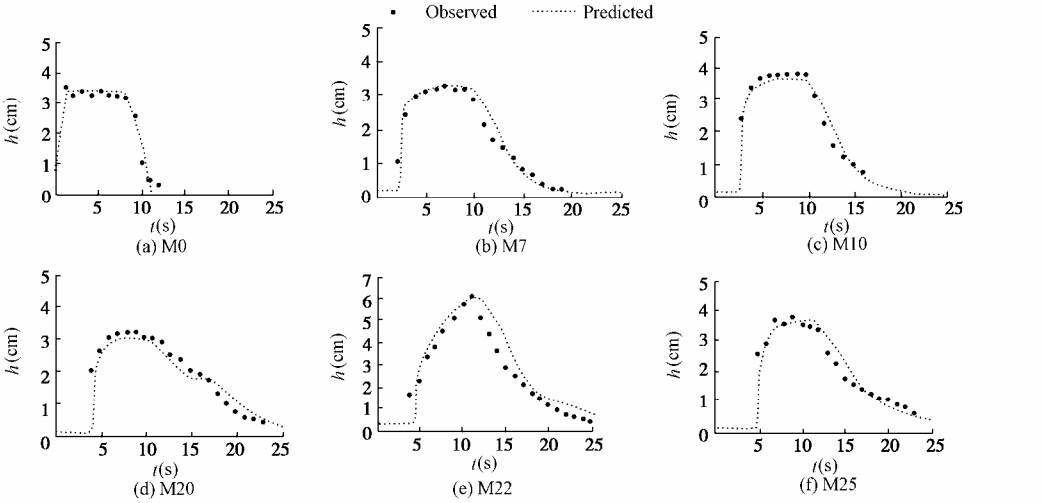

Fig. 15 Comparison of observed and predicted depths of unsteady flow at six measurement points (pipe slope of 1/50)

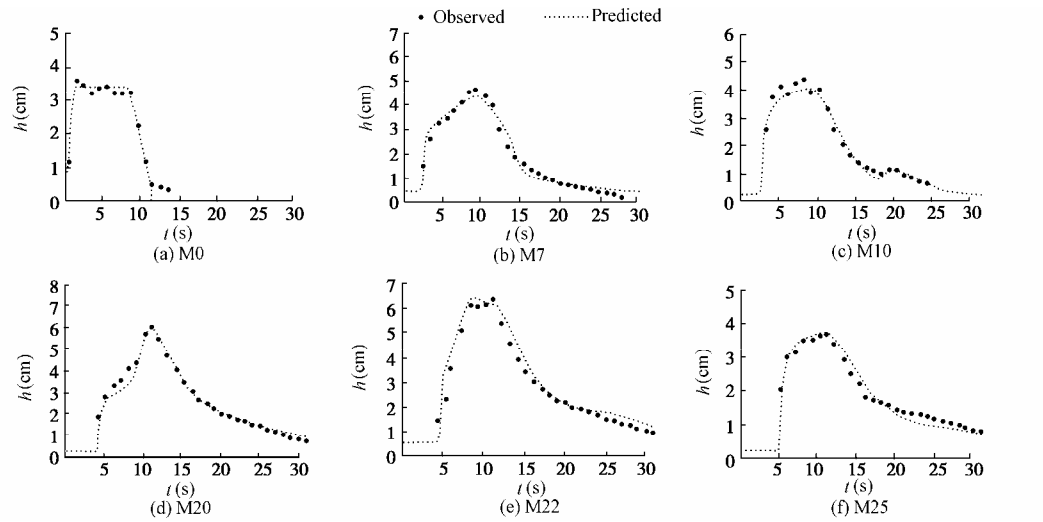

Fig. 16 Comparison of observed and predicted depths of unsteady flow at six measurement points (pipe slope of 1/100)

6 Application to pipe flow including junctions and bends

The numerical model was applied to a practical drainage situation that included multiple discharge inputs, junctions and bends. The experimental device and conditions are shown in Fig. 17. A steady flow rate of 0.5 L/s was applied to the main pipe, and WC(B) was discharged two seconds after the discharge of WC(A). Flow depth data were obtained at the eight measurement points from M1 to M8 shown in Fig. 17(c).

The flow network was divided into five pipe elements (two branch pipe sections, a pipe

section with a bend, a main pipe section between two junctions, and a main pipe section between the inflow cross section and first junction). Combining the junction model and bend model described above, the numerical model can be used to model the flow network. Comparison of calculated and measured flow depths at six typical measurement points is shown in Fig. 18. The simulated water depth at M2 is somewhat high after discharge of WC(A), and this seems to affect the calculated results at M7 and M8, downstream of M6. In other aspects, however, the calculated results match the experimental results fairly well. Since the second peak observed at M7 is caused by the backflow from discharge of WC(A), the junction model may not be appropriate for this type of flow behavior. The junction model should be refined so as to improve the quality of prediction.

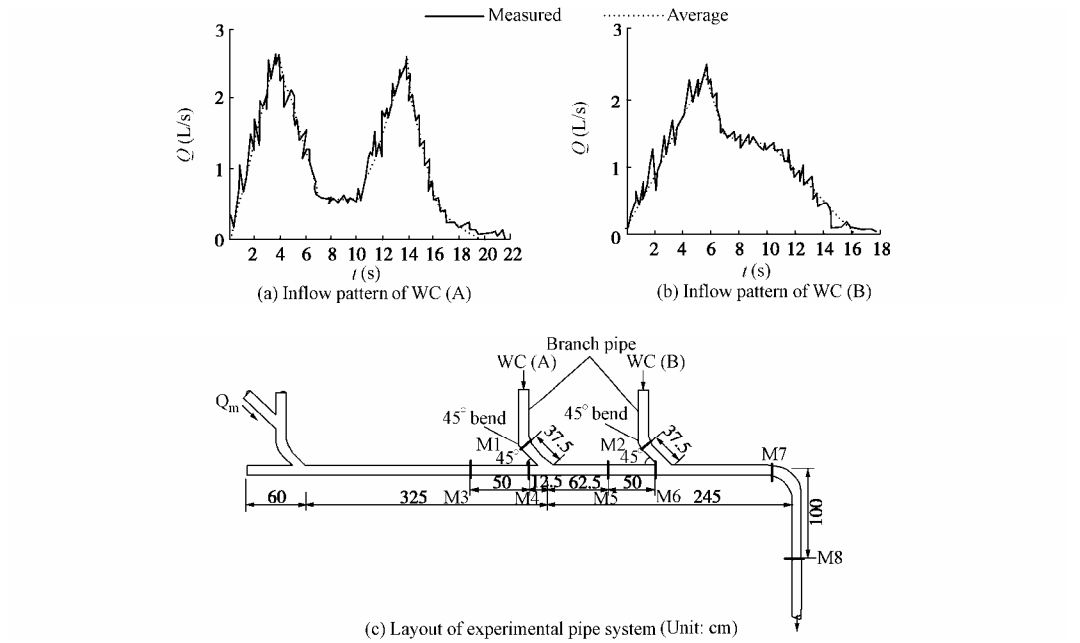

Fig. 17 Sketch of experimental device and conditions of model including junctions and bends

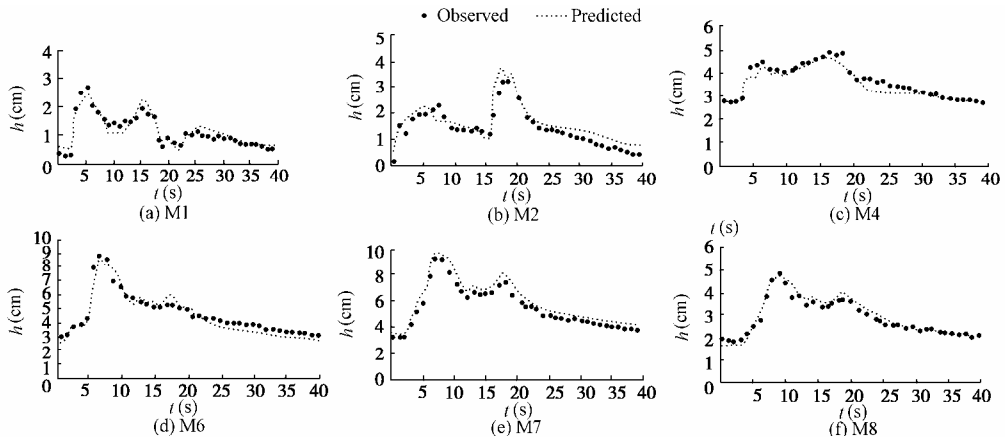

Fig. 18 Comparison of observed and predicted depths at six measurement points

7 Conclusions

A numerical model for simulating transient flow in horizontal drainage networks using the characteristics method with time-line interpolation was presented. The junction and bend models were developed based on the steady-state experimental results, and were found to reproduce the observed flow depth profiles under simplified flow conditions fairly well. The reproduced features include backwater profiles upstream of the junction and bend as well as the rapid acceleration of the flow. The application of the numerical model to a practical situation has shown that many of the complicated flow features can be simulated realistically.

More comparative studies of simulations and experiments will be needed to apply various pipe patterns into various actual drainage configurations. The presented numerical model also needs to be expanded to include top-entry junction models based on detailed measurements.

References

Mao, Z. Y. 1993. *Partially Filled Unsteady Flow Analysis in the Region of Pipe Junctions*. Ph. D. Dissertation. Edinburgh: Heriot-Watt University.

Mao, Z. Y. 1995. A new approach to the simulation of unsteady subcritical flow. *Journal of Hydrodynamics, Ser. B*, 7(3), 84-93.

Mao, Z. Y. 1996a. Comprehensive study of combining flow conditions at pipe junctions. *Journal of Hydrodynamics, Ser. B*, 8(1), 76-84.

Mao, Z. Y. 1996b. A mathematical model of unsteady flow in the multistory drainage network. *Journal of Hydrodynamics, Ser. A*, 11(2), 127-132. (in Chinese).

Mao, Z. Y. 1996c. Numerical simulation of discontinuous flow in circular conduits. *Journal of Hydrodynamics, Ser. B*, 8(3), 64-74.

Mao, Z. Y., and Chen, C. Z. 1997. Computer-aided analysis of unsteady partially filled flows in drainage systems. *Journal of Hydrodynamics, Ser. B*, 9(4), 46-53.

Mao, Z. Y., Wang, J. L., and Zhao, X. 2004. Simulation of transient flow in building drainage networks. *Proceedings of 4th International Symposium on Environmental Hydraulics and 14th IAHR-APD Congress*, 2, 1371-1378. Hong Kong: CRC Press.

She, Y. T., and Mao, Z. Y. 2003. Flow simulation of urban sewer networks. *Tsinghua Science and Technology*, 8(6), 719-725.

Swaffield, J. A., and Galowin, L. S. 1992. *The Engineered Design of Building Drainage Systems*. Cambridge: Ashgate Publishing Limited.